Journal of Controlled Release 336 (2021) 469–479

Contents lists available at ScienceDirect

Journal of Controlled Release

journal homepage: www.elsevier.com/locate/jconrel

Self-assembled micelle responsive to quick NIR light irradiation for fast drug release and highly efficient cancer therapy

Yue Zhang [a,c], Xiaobo Zhang [a], Weiwei Chen [a], Yuling He [a], Ying Liu [a,b,*], Huangxian Ju [a,*]

[a] State Key Laboratory of Analytical Chemistry for Life Science, School of Chemistry and Chemical Engineering, Nanjing University, Nanjing 210023, China
[b] Chemistry and Biomedicine Innovation Center, Nanjing University, Nanjing 210023, China
[c] School of Pharmacy, Nanjing University of Chinese Medicine, Nanjing 210023, China

ARTICLE INFO

Keywords:
Upconversion nanoparticles
Drug delivery
Photo responsive
Micelle
Cancer therapy

ABSTRACT

Upconversion nanoparticles (UCNPs) have been used for designing near infrared (NIR) light-responsive nanocarriers and controllable drug release. However, the need for long-term NIR light irradiation over hours impaired their application efficiency. Here we develop a self-assembled micelle of amphipathic polymer P-DASA which degrades *via* quick NIR light irradiation. UCNPs and DOX are also encapsulated in the micelle for quick drug release. P-DASA is composed of hydrophilic polyethylene glycol segment and photo-responsive hydrophobic donor–acceptor Stenhouse adduct (DASA). Only 5-min NIR irradiation causes the hydrophilicity conversion of P-DASA and the complete disruption of micelle with DOX fast release of 83.7% in 30 min to achieve highly efficient therapy. Moreover, the P-glycoprotein mediated DOX efflux is also diminished by concomitantly producing NO intracellularly. This micelle demonstrates impressive *in vivo* therapeutic effect, and thus provides an avenue for highly efficient cancer therapy.

1. Introduction

Self-assembled micelle possess hydrophobic interior and hydrophilic outward surface, are thus ideal drug delivery carriers with significant merits for drug loading and long-term circulation [1,2]. Some micelle-based formulations have entered the clinical trial stages [3,4]. Through incorporation of stimuli-responsive moieties into the polymer branches, controlled micelle disruption with corresponding cargo release has been achieved *via* chemical bond cleavage, isomerization or solubility changes under various stimuli [5–8]. As a type of external stimulus, light irradiation provides remote activation with high spatio-temporal control for the release of loaded drug, which avoids off-target damage and enhances therapeutic efficacy [9], therefore has attracted wide attention in biomedicine [10].

Near-infrared (NIR) light has deeper penetration into tissues and is less detrimental to healthy cells [11,12]. Tm^{3+}-doped upconversion nanoparticles (UCNPs) absorb NIR light and emit higher-energy photons in UV regions. Li research group combined UCNPs with functional DNA strands and structures, and achieved precise spatiotemporal control for intracellular sensing of pH [13], RNAs [14,15], and ATP [16] for the first time, as well as regulation drug release/therapy activation [17,18]. UCNPs were also conjugated to self-assembled micelles with UV responsive molecules including *o*-nitrobenzyl [19], azobenzene [20] and spiropyran [21] to achieve NIR light controlled drug release. However, the transition of electrons to higher energy excited state $^1D_2$ is rare for Tm^{3+} doped UCNPs, which lowers the quantum yield of UV emission from $^1D_2 \rightarrow {}^3H_6$ transition below 1% [22,23]. Therefore, the NIR light-responsive drug release based on Tm^{3+} doped UCNPs is usually sluggish. To reach desirable drug release concentration, continuous NIR light irradiation over several hours is usually required [19–21,24], which inconveniences therapeutic process, causes thermal injuries to healthy tissues, and would impair therapeutic efficiency. Therefore, the design of drug quick release strategy in response to short time NIR light exposure is of great urgency.

Er^{3+} doped UCNPs can produce visible emission at 541 nm *via* electron transition of $^4S_{3/2} \rightarrow {}^4I_{15/2}$ with a quantum yield of 3.36 ± 0.06% [25]. Compared with Tm^{3+} doped UCNPs, Er^{3+} doped UCNPs is more powerful in converting NIR light to shorter wavelength light, and have been used for activating photosensitizers [26] in photodynamic therapy (PDT) [27,28]. Here we used Er^{3+} doped UCNPs to trigger the structure conversion of donor–acceptor Stenhouse adduct (DASA) from hydrophobic to hydrophilic [29,30], which resulted the quick disruption

* Corresponding authors at: State Key Laboratory of Analytical Chemistry for Life Science, School of Chemistry and Chemical Engineering, Nanjing University, Nanjing 210023, China.
E-mail addresses: yingliu@nju.edu.cn (Y. Liu), hxju@nju.edu.cn (H. Ju).

https://doi.org/10.1016/j.jconrel.2021.06.028
Received 27 February 2021; Received in revised form 8 June 2021; Accepted 20 June 2021
Available online 23 June 2021

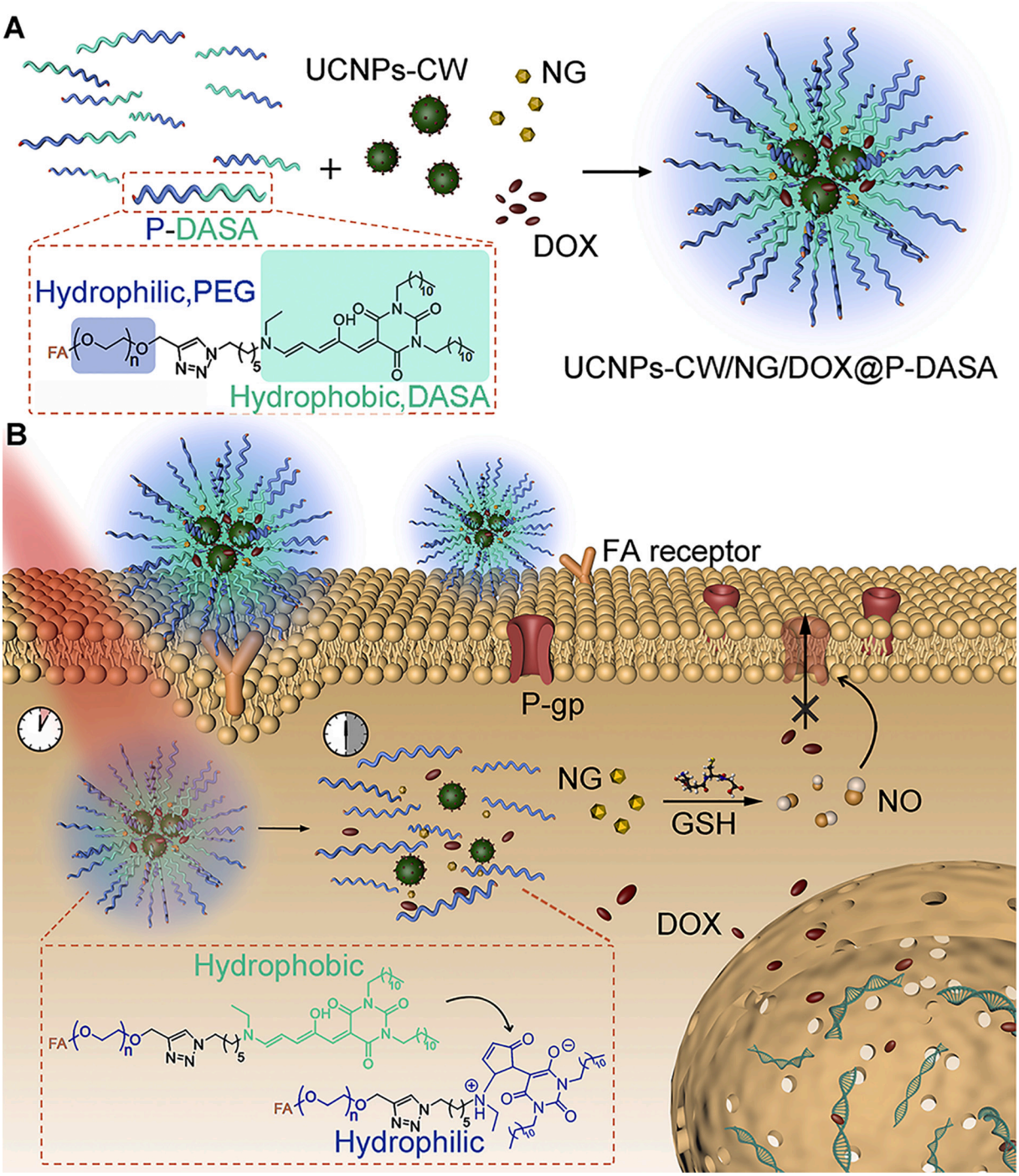

Scheme 1. (A) Self-assembly of UCNPs-CW/NG/DOX@P-DASA (B) NIR light-ignited fast disruption of the micelle for quick DOX release and NO generation.

of self-assembled micelle in response to fast NIR exposure of 5 min with rapid and efficient release of loaded drug. Amphipathic polymer branches P-DASA was synthesized by linking hydrophilic polyethylene glycol (PEG) to hydrophobic DASA. UCNPs were modified with IRDye® 800CW as antenna (UCNPs-CW) to enhance the upconversion luminescence efficiency [31]. P-DASA was self-assembled with UCNPs-CW, anticancer drug doxorubicin (DOX), and nitroglycerin (NG) to prepare micelle UCNPs-CW/NG/DOX@P-DASA that is responsive to NIR light fast irradiation (Scheme 1A). After endocytosis and short time NIR light irradiation, upconversion emission of UCNPs-CW at 541 nm triggered photochemical reaction of DASA with configuration transition from hydrophobic to hydrophilic, which resulted the fast and complete disintegration of micelle with sufficient DOX release in 30 min. NG worked as NO donor [32,33] to produce NO intracellularly by reacting with glutathione (GSH) overexpressed in most tumor cells [34] upon the disruption of micelle, which inhibited P-glycoprotein mediated drug efflux in tumor cells [34–36] (Scheme 1B). This design of micelle quick disruption greatly shortened the NIR irradiation time from several hours for most UCNPs-based therapy strategies to 5 min, and therefore would highly facilitate therapeutic process and avoid thermal injuries. Therefore, the proposed drug delivery system with short NIR light irradiation time, rapid drug release capability and high therapeutic efficiency provides convenient and efficient clinical therapeutic approaches.

2. Materials and methods

2.1. Materials and apparatus

Anhydrous ytterbium chloride ($YbCl_3$), anhydrous yttrium chloride (YCl_3), anhydrous gadolinium chloride ($GdCl_3$), anhydrous erbium chloride ($ErCl_3$), anhydrous neodymium chloride ($NdCl_3$), oleic acid (OA), 1-octadecene (ODE), doxorubicin (DOX), 1% (*w*/w) nitroglycerin (NG), genistein, wortmannin, and 4-amino-5-methylamino-2′,7′-difluorescein (DAF-FM) were purchased from Sigma-Aldrich (USA). Fetal bovine serum (FBS) was from Thermo Fisher Scientific (USA). Folate and alkynyl labelled polyethylene glycol (FA-PEG-alkynyl) (5000 kD) was obtained from ToYongBio Tech. Inc. (Shanghai, China). 6-Azido-N-ethylhexan-1-amine was received from Finetech Industry Limited (UK). Ammonium fluoride (NH_4F), sodium hydroxide (NaOH), alendronic acid (ADA), methanol, trichloromethane ($CHCl_3$), acetone, hydrochloric acid (HCl), ethyl alcohol, N-hydroxysuccinimide (NHS), 1-ethyl-3-(3-dimethylaminopropyl) carbodiimide-HCl (EDC), sucrose, NaN_3, folic acid (FA), octanoic acid, tetrahydrofuran (THF), n-dodecyl amine, dichloromethane (CH_2Cl_2), n-dodecyl isocyanate, malonyl chloride, $MgSO_4$, hexane, ethyl acetate (EtOAc), pyrene, 2-furaldehyde, $CuSO_4{\cdot}5H_2O$, sodium ascorbate, diethyl ether, and glutathione (GSH) were purchased from Aladin Ltd. (Shanghai, China). NHS-IRDye® 800CW was obtained from LI-COR (Lincoln, Nebraska, USA). NHS-Cy3 was purchased from Fanbo Biochemicals (Beijing, China). P-glycoprotein (P-gp) ELISA kit was from Jinyibai Biological Technology (Nanjing, China). 4′,6-Diamidino-2-phenylindole (DAPI), Annexin V FITC/PI apoptosis detection kit, DAF-FM diacetate, nitric oxide (NO) detection kit, MTT cell proliferation and cytotoxicity detection kit, and phosphate buffered saline (PBS) (10 mM, pH 7.4) were from Keygen Biotech (Nanjing, China). Hematoxylin-eosin staining kit was obtained from Beyotime Biotechnology (Shanghai, China).

Transmission electron microscopic (TEM) images were captured on JEM-2800 transmission electron microscope (JEOL Ltd., Japan) by dropping 10 μL samples on carbon supported membrane (ZhongJing KeYi Technology Co., Ltd., China). The fluorescence spectra were obtained on FluoroMax-4 spectrofluorophotometer (HITACHI, Japan) with an additional continuous-wave laser (808 nm). Powder X-ray diffraction (XRD) analysis was conducted on ARL X'TRA XRD system (Thermo Fisher Scientific, USA). Dynamic light scattering (DLS) analysis was performed on ZetaPlus 90 Plus/BI-MAS (Brook haven, USA). The UV–Vis absorption spectra and the light transmittances were acquired on an optical spectrophotometer equipped with DH-2000 UV–Vis-NIR light source and Maya 2000 Pro detector (Ocean Optics, China). Nuclear magnetic resonance (NMR) spectra were obtained on a Bruker DPX 400 MHz spectrometer. Green light irradiation was conducted using a 532-nm laser (50 mW cm^{-2}) (Lasever Inc., China). The cell images were acquired on TCS SP5 confocal laser scanning microscope (CLSM) (Leica, Germany). Flow cytometric analysis was performed on Coulter FC500 flow cytometer (Beckman-Coulter, USA). MTT and ELISA assays were performed on Hitachi/Roche System Cobas 6000 (Bio-Rad, USA).

2.2. Synthesis of UCNPs

The UCNPs were synthesized according to our previous work [31]. 0.9 mmol YCl_3 and 0.1 mmol $GdCl_3$ were mixed with 5 mL OA and 15 mL ODE, and heated to 150 °C under vacuum for 60 min. After cooling to 45 °C, the mixture was added with 10 mL methanol solution of NH_4F (148 mg) and NaOH (100 mg) dropwise and continuously reacted for 30 min. The reaction solution was then heated to 110 °C for 15 min and 300 °C for 90 min under nitrogen to obtain the core ($NaYF_4$:Gd).

To prepare the precursor of emitting layer, 0.663 mmol YCl_3, 0.17 mmol $YbCl_3$ and 0.017 mmol $ErCl_3$ were mixed with 2 mL OA and 6 mL ODE, and heated to 150 °C for 1 h under vacuum. The reaction solution was then cooled down to 45 °C, added with 8.5 mL methanol solution containing 125.8 mg NH_4F and 85.0 mg NaOH dropwise. After 30-min reaction, the mixture was heated to 110 °C for 15 min to remove methanol, and the obtained precursor of emitting layer was kept at 110 °C under nitrogen for further use. Meanwhile, the precursor of absorption shell was prepared using the same method with 0.60 mmol $LnCl_3$ (Y:Yb:Nd = 60:10:30) and 6 mL methanol solution containing 88.8 mg NH_4F and 60.0 mg NaOH.

The emitting layer was grown by injecting 8 mL emitting layer precursor into the reaction solution of core and stirring at 300 °C for 30 min to get $NaYF_4$:Gd@$NaYF_4$:Yb,Er. Afterwards, 8 mL absorption shell precursor was injected and reacted for 30 min at 300 °C to grow the absorption layer. The as-prepared UCNPs ($NaYF_4$:Gd@$NaYF_4$:Er,Yb@$NaYF_4$:Yb,Nd) were precipitated with acetone, and re-dispersed in $CHCl_3$ at 20 mg mL^{-1} for further use.

2.3. Modification of UCNPs with 800CW

The UCNPs were first ligand-exchanged with ADA for surface functionalization with amine groups. 50 mg ADA, 6 mL water and 4 mL ethyl alcohol were added in 10 mL $CHCl_3$ containing 20 mg mL^{-1} UCNPs, and the mixture was adjusted to pH 2.0 with HCl (1 M). After stirring for 30 min at room temperature, the upper aqueous solution was collected, washed with water repeatedly and re-dispersed in 10 mL water to get UCNPs-ADA.

5 mL 1 mg mL^{-1} UCNPs-ADA was then mixed with 3 μL 0.5 mM NHS-IRDye® 800CW and stirred overnight at room temperature. The nanoparticles were centrifuged and re-dispersed in 5 mL THF (solution A). To increase the nanoparticle hydrophobicity, 2 μL octanoic acid was dispersed in 300 μL THF, activated *via* 2-h incubation with 100 μL EDC (0.1 M) and 100 μL NHS (0.1 M), and subsequently mixed with 5 mL solution A and stirred for 8 h at room temperature. The as-obtained UCNPs-CW with desired hydrophobicity were centrifuged, washed with THF and re-dispersed in 5 mL THF.

Cy3 labelled UCNPs-CW ($UCNPs_{Cy3}$-CW) were synthesized through the similar method except that 5 μL 30 mM NHS-Cy3 was added along with 3 μL 0.5 mM NHS-IRDye® 800CW in 5 mL 1 mg mL^{-1} UCNPs-ADA.

2.4. Synthesis of UCNPs-CW/NG/DOX encapsulated micelle (UCNPs-CW/NG/DOX@P-DASA)

2 mg P-DASA was dispersed in 2.7 mL THF, and mixed with 1 mg UCNPs-CW, 100 μL 0.4 mg mL^{-1} DOX and 200 μL 0.2 mg mL^{-1} NG. After ultrasonically dispersed for 20 min, the mixture was added into 60 mL water dropwise and stirred for 8 h at 37 °C. The obtained UCNPs-CW/NG/DOX@P-DASA micelle were collected through centrifugation (4000 r, 5 min) and re-dispersed in 2 mL water.

DOX@P-DASA, NG@P-DASA, UCNPs-CW/DOX@P-DASA, UCNPs-CW/NG@P-DASA and $UCNPs_{Cy3}$@P-DASA were synthesized according to the same process in the absence of UCNPs, NG or DOX, or in the presence of $UCNPs_{Cy3}$ instead of UCNPs.

The critical micelle concentration (CMC) was measured by using pyrene as the probe. The P-DASA solutions with different concentrations were mixed with pyrene (0.6 mg mL^{-1}), vibrated for 1 h, and incubated overnight. The ratio of pyrene fluorescence intensities at 338 nm and 333 nm (I_{338}/I_{333}) was recorded.

2.5. In vitro verification of DOX release and NO generation

500 μg mL^{-1} UCNPs-CW/DOX@P-DASA or DOX@P-DASA was irradiated with 808-nm laser (2 W cm^{-2}) for 5 min, and the fluorescence of DOX in the supernatants was detected at different times under 480-nm excitation to obtain the release percentages of DOX. Samples without NIR irradiation were also detected as controls.

500 μg mL^{-1} UCNPs-CW/NG@P-DASA or NG@P-DASA was mixed with 50 μM DAF-FM and 10 mM GSH. The mixture was then irradiated with 808-nm laser (2 W cm^{-2}) for 5 min and the fluorescence spectra of DAF-FM in the supernatant were obtained under 495-nm excitation at

different times. Samples without NIR irradiation or GSH were also detected as controls. Quantification of NO was achieved using NO detection kit according to the instruction procedure. The NO generation of UCNPs-CW/NG/DOX@P-DASA was also detected using NO detection kit.

2.6. Stability assay

1 mg mL^{-1} UCNPs-CW/NG/DOX@P-DASA micelle was dispersed in PBS and PBS containing 10% FBS respectively and incubated at 37 °C for 24 h to monitor the hydration size and polymer dispersity index. In addition, the leakage of DOX in FBS buffer was detected during 12-h incubation.

2.7. Cell culture

MCF-10a cells (Keygen Biotech, China) and DOX-resistant MCF-7/ADR cells (Shanghai Meixuan Biological Technology, China) were cultured in RPMI 1640 medium supplemented with 10% FBS and 1% penicillin-streptomycin solution (100 μg mL^{-1}) at 37 °C in a humidified atmosphere containing 5% CO_2. The cell numbers were detected using Countess® II automated cell counter (Invitrogen, USA).

2.8. CLSM imaging of treated cells

For verification of intracellular delivery specificity, 1×10^4 MCF-7/ADR cells or MCF-10a cells were seeded into a glass dish and treated with 300 μg mL^{-1} micelle at 37 °C for 6 h. After washing with PBS, the fluorescence of UCNPs-CW was measured from 600 to 700 nm under 808-nm excitation. UCNPs-CW fluorescence was also measured from FA pretreated MCF-7/ADR cells after incubated with 300 μg mL^{-1} micelle.

For DOX and UCNPs co-localization imaging, the micelle treated MCF-7/ADR cells were irradiated with 808-nm laser (2 W cm^{-2}) for 5 min. After 25-min incubation at 37 °C, the cells were stained with 5 μg mL^{-1} DAPI for 10 min, and the fluorescence signals were collected from 600 to 700 nm under 808-nm excitation for UCNPs-CW, from 550 to 650 nm under 488-nm excitation for DOX and from 450 to 500 nm under 405-nm excitation for DAPI.

The intracellular NO generation was verified by incubating MCF-7/ADR cells with 300 μg mL^{-1} micelle or UCNPs-CW/DOX@P-DASA for 6 h, and then staining with 5 μM DAF-FM diacetate for 20 min. After washing with PBS for three times, the cells were irradiated with 808-nm laser (2 W cm^{-2}) for 5 min to incubate for 25 min at 37 °C. The fluorescence signals were collected from 500 to 550 nm under 488-nm excitation.

2.9. Endocytosis pathway examination

MCF-7/ADR cells were preincubated with 200 mg mL^{-1} genistein, 50 nM wortmannin, 450 nM sucrose or 10 mM NaN_3 for 30 min and then treated with $UCNPs_{Cy3}$-CW@P-DASA for 6 h to perform flow cytometric analysis.

2.10. Cytotoxicity assay

After MCF-7/ADR cells were cultured in 96-well plate (1×10^4 cells/well) for 12 h, different concentrations of the micelle were added to incubate for 6 h. After washing with PBS, the cell viabilities were detected with MTT assay according to the instruction procedure.

2.11. Cell proliferation and apoptosis assay

MCF-7/ADR cells were incubated with 300 μg mL^{-1} UCNPs-CW@P-DASA, UCNPs-CW/NG@P-DASA, UCNPs-CW/DOX@P-DASA, UCNPs-CW/NG/DOX@ P-DASA or 3.75 μg mL^{-1} DOX for 6 h and irradiated with 808-nm light (2 W cm^{-2}) for 5 min. After the cells were further cultured for 24 h, the cell proliferation and apoptosis were analyzed with MTT assay and flow cytometry, respectively. Annexin V-FITC/PI apoptosis detection kit was utilized for cell stain in flow cytometric analysis.

2.12. Detection of P-gp expression

MCF-7/ADR cells were incubated with 3.75 μg mL^{-1} DOX, 300 μg mL^{-1} UCNPs-CW/DOX@P-DASA or the micelle for 6 h and washed with PBS. After irradiation with 808-nm light (2 W cm^{-2}) for 5 min, the cells were further cultured for 12 h to detect the expression levels of P-gp with ELISA kit according to the instruction procedure.

2.13. Detection of intracellular DOX accumulation

After incubating MCF-7/ADR cells with 3.75 μg mL^{-1} DOX, 300 μg mL^{-1} UCNPs-CW/DOX@P-DASA or the micelle for 6 h, they were irradiated with 808-nm light (2 W cm^{-2}) for 5 min, and further cultured for 6 h to collect the fluorescence of DOX with flow cytometer.

2.14. In vivo imaging and antitumor efficiency

Pathogen-free female BALB/c nude mice (5–6 weeks) (Keygen Biotech, China) were used to verify the *in vivo* antitumor efficiency of the micelle. All mice had liberated access to water and rodent chow. All experiments were conducted according to the Institutional Animal Use and Care Regulations approved by the Model Animal Research Center of Nanjing University (MARC, No. 190836). 1.0×10^6 MCF-7/ADR cells were inoculated subcutaneously into the right armpit of the mice to establish a MCF-7/ADR tumor xenograft mouse model. The tumor volumes were calculated with formula $V = (L \times W^2)/2$, where W and L are the width and length of the tumor respectively.

To evaluate the biodistribution of $UCNPs_{Cy3}$-CW@P-DASA, the tumor-bearing mice were intravenously injected with 150 μL of 300 μg mL^{-1} $UCNPs_{Cy3}$-CW@P-DASA or $UCNPs_{Cy3}$-CW@P-DASA' (in the absence of targeting group FA) and imaged at different times on the IVIS Lumina XR III *in vivo* imaging system (PerkinElmer, USA).

For *in vivo* antitumor efficiency investigation, when the tumors grew to 80 mm^3, the mice were divided into 8 groups randomly and different groups were intravenously injected with 150 μL of (1,2) saline, (3,4) UCNPs-CW/DOX@P-DASA (300 μg mL^{-1}), (5,6) the micelle (300 μg mL^{-1}), (7,8) DOX (3.75 μg mL^{-1}). At 4 h after injection, the tumors of the mice in groups (2), (4), (6) and (8) were irradiated with 808-nm laser (1 W cm^{-2}) for 5 min, while groups (1), (3), (5) and (7) in the absence of NIR light irradiation were set as controls. The injection and irradiation were performed at Day 3 and Day 6 repeatedly, and the tumor sizes and weight of all mice were recorded every 2 days. At Day 14, all the mice were euthanized to take the representative photos. Besides, the tumors in the mice were collected, washed with PBS, and immersed in 4% paraformaldehyde solution to conduct hematoxylin-eosin staining according to the instruction procedure. For groups (1) and (6), the major organs (heart, kidney, spleen, lung and liver) were collected to perform the histopathological analysis with the same procedure.

3. Results and discussion

3.1. Preparation of UCNPs-CW@P-DASA and NIR light-responsive disassembly

The UCNPs ($NaYF_4$:Gd@$NaYF_4$:Er,Yb@$NaYF_4$:Yb,Nd) possessed a core/shell/shell structure and were synthesized according to our previous work [31] as shown in Fig. S1. Nd^{3+} and Yb^{3+} were co-doped in the outer shell $NaYF_4$:Yb,Nd to absorb NIR excitation at 808 nm [37] and transfer the energy inward to Er^{3+}/Yb^{3+} co-doped inner shell $NaYF_4$:Er,Yb for upconversion luminescence with peaks at 541 nm and 655 nm (Fig. S2A). The transmission electron microscopic (TEM) images

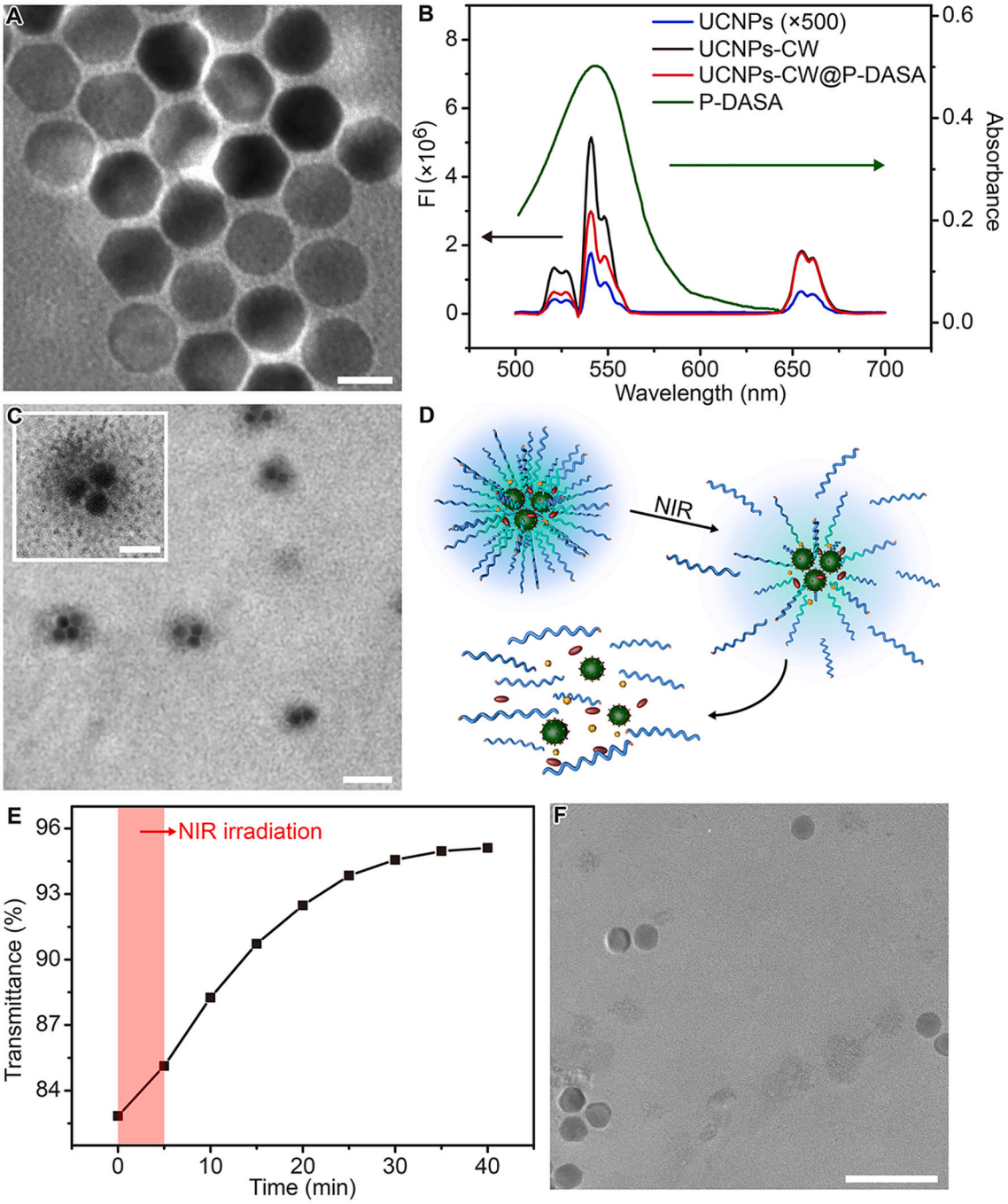

Fig. 1. (A) TEM image of $NaYF_4$:Gd@$NaYF_4$:Er,Yb@$NaYF_4$:Yb,Nd with the scale bar of 30 nm. (B) Upconversion luminescence spectra of UCNPs, UCNPs-CW, UCNPs-CW@P-DASA and UV–Vis absorption spectrum of P-DASA. (C) TEM image of UCNPs-CW@P-DASA with the scale bar of 150 nm (inset: 75 nm). (D) Schematic illutration of UCNPs-CW@P-DASA disassembly process. (E) Time dependent light transmittances at 660 nm for 500 μg mL^{-1} UCNPs-CW@P-DASA after 5-min NIR irradiation. (F) TEM image of UCNPs-CW@P-DASA at 25 min after 5-min NIR irradiation. The scale bar is 150 nm.

showed a uniform size of 25 nm for $NaYF_4$:Gd core (Fig. S2B), the thickness of ~4.0 nm for the emitting shell $NaYF_4$:Er,Yb (Fig. S2C), and the thickness of ~3.5 nm for the absorption shell of UCNPs (Fig. 1A), respectively. Powder X-ray diffraction (XRD) patterns verified that the $NaYF_4$:Gd, $NaYF_4$:Gd@$NaYF_4$:Er,Yb and UCNPs were all hexagonal nanocrystals (Fig. S2D). UCNPs surface was then modified with ADA and covalently immobilized with antenna molecule IRDye® 800CW (Fig. S1), The upconversion luminescence intensity of the as-synthesized UCNPs-CW greatly increased due to the strong ability of 800CW to harvest 808-nm light [31] (Fig. 1B), which resulted in 1450 times stronger luminescence intensity at 541 nm than that of UCNPs.

As the component for micelle assembly, amphipathic polymer P-DASA was synthesized *via* click reaction (see the detailed synthetic process in the Supplementary Materials), and confirmed by ^{1}H NMR spectra (Fig. S3A-D). The P-DASA showed a UV–Vis absorption peak at 542 nm, which was well matched with the emission peak of UCNPs-CW at 541 nm under 808-nm exposure (Fig. 1B). After irradiation for 5 min, the ^{1}H NMR spectra change of DASA (Fig. S3E and S3F) and significantly decreased absorption peak of P-DASA (Fig. S4A) indicated the photo-responsive structure change of DASA segment, which led to the conversion of P-DASA from hydrophobic to hydrophilic [38]. This guaranteed the response of P-DASA to NIR irradiation with the conjugation of

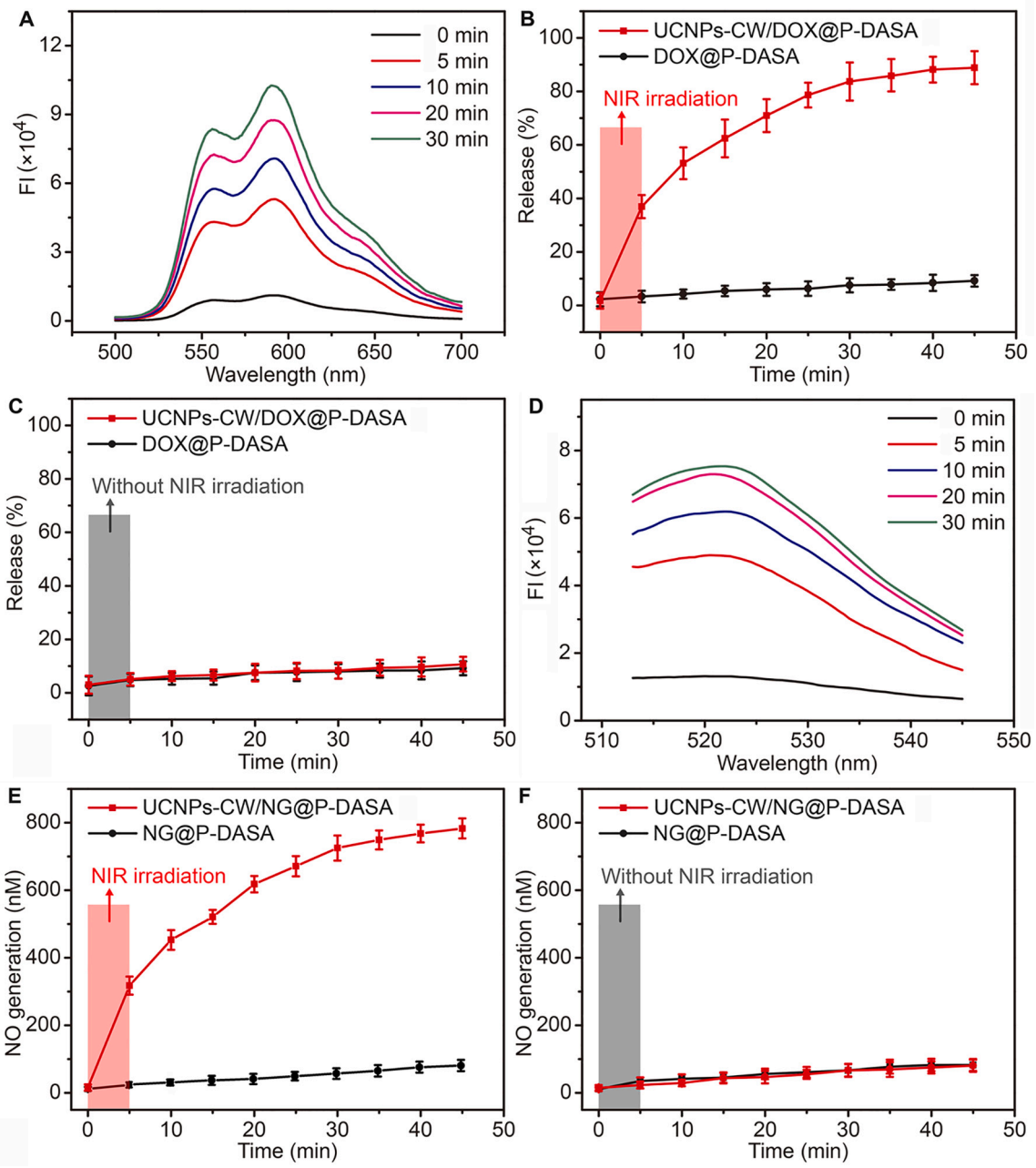

Fig. 2. (A) Time dependetn fluorescence spectra for supernatants of UCNPs-CW/DOX@P-DASA after 5-min NIR irradation. (B,C) Release percentages of DOX from UCNPs-CW/DOX@P-DASA or DOX@P-DASA with (B) and without (C) 5-min NIR irradiation. (D) Time dependetn fluorescence spectra for supernatants of 500 μg mL^{-1} UCNPs-CW/NG@P-DASA containing 50 μM DAF-FM and 10 mM GSH after 5-min NIR irradiation. (E,F) Quantification of NO generation from UCNPs-CW/NG@P-DASA or NG@P-DASA with (E) and without (F) 5-min NIR irradiation. The data error bars indicate means ± SD ($n = 3$).

UCNPs.

After UCNPs-CW and P-DASA were dispersed in THF and added into water dropwise, the micelle (UCNPs-CW@P-DASA) was self-assembled with a diameter of ~120 nm and 2–4 UCNPs-CW encapsulated in the center (Fig. 1C). Its hydrodynamic diameter was 138 nm with polydispersity index (PDI) of 0.041 (Fig. S4B). The critical micelle concentration (CMC) of P-DASAwas calculated as 25 μg mL^{-1} using pyrene as the probe (Fig. S4C). Under 808-nm light irradiation, UCNPs-CW@P-DASA micelle showed the same luminescence intensity as UCNPs-CW for 655 nm emission peak, but the luminescence intensity at 541 nm decreased due to the absorbance DASA in hydrophobic state (Fig. 1B). With the increasing irradiation time of 808-nm light up to 5 min, the absorption of P-DASA rapidly decreased (Fig. S4D and S4E), indicating the continuous conversion of DASA to hydrophilic state. Hydrophilicity conversion of DASA caused the disassembly of P-DASA with the quick disruption of micelle (Fig. 1D). The disassembly of UCNPs-CW@P-DASA was confirmed by the increasing light transmittance from 83.5% to 94.6% in 30 min (Fig. 1E) and the disappearance of micellar structure in TEM image (Fig. 1F). Thus UCNPs-CW@P-DASA could be used as a NIR light fast ignited micelle for quick drug release.

3.2. DOX release and NO generation from UCNPs-CW/NG/DOX@P-DASA

Doxorubicin (DOX), as a model hydrophobic drug, could be encapsulated in the hydrophobic core of UCNPs-CW@P-DASA during the self-assembly process, which was demonstrated by fluorescent characteristic peak of DOX at 592 nm (Fig. S5A). The loading capacity of DOX in

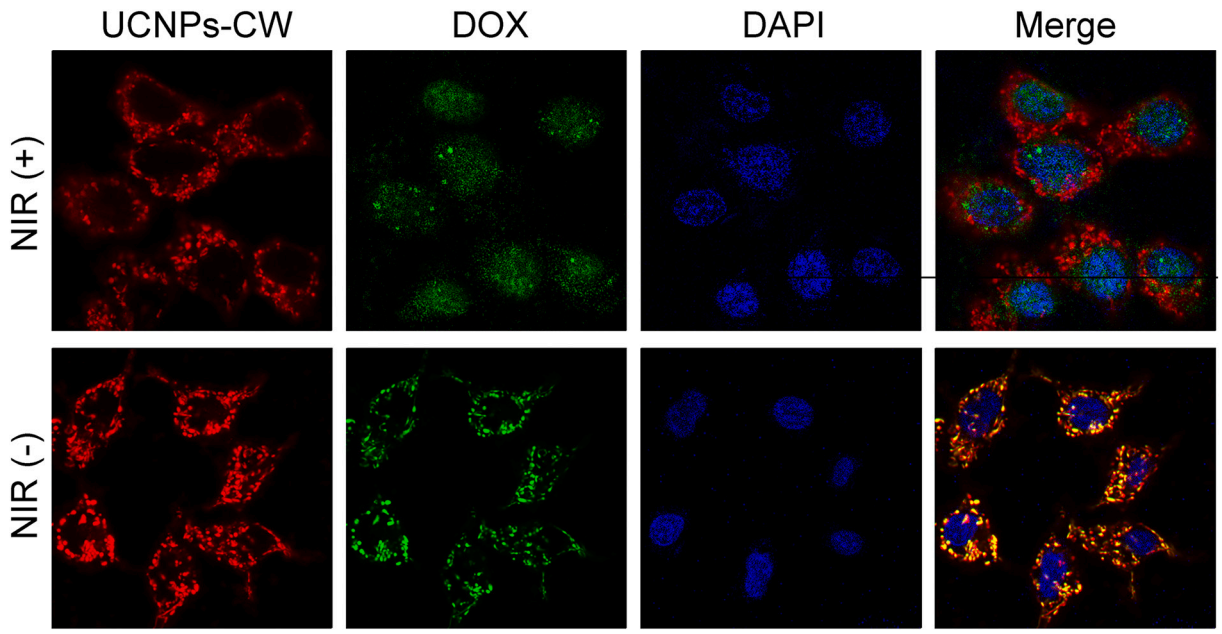

Fig. 3. CLSM images of the micelle treated MCF-7/ADR cells after 5 min NIR irradiation (NIR (+)) or without NIR irradiation (NIR (−)) with continuous 25-min incubation in cell culture media (scale bar: 25 μm).

UCNPs-CW/DOX@P-DASA was calculated as 12.5 μg mg^{-1} (Fig. S5A and S5B). To monitor the release of DOX from UCNPs-CW/DOX@P-DASA, the micelle was irradiated under 808-nm light for 5 min, and the supernatants were collected at different times to measure the fluorescence intensities of DOX (Fig. 2A). The release percentage of DOX showed a dramatic rise in response to 5-min NIR irradiation and saturated at 83.7% in 30 min (Fig. 2B, red line). The impressive DOX release efficiency was due to the complete disassembly of micelle upon NIR exposure (Fig. 1E, F). In comparison, little leakage of DOX from UCNPs-CW/DOX@P-DASA was observed in the absence of NIR irradiation (Fig. S5C; Fig. 2C, red line). Moreover, DOX@P-DASA also showed little leakage of DOX in both the presence and the absence of NIR irradiation (Fig. 2B and Fig. 2C, black line; Fig. S5D and Fig. S5E), indicating the key roles of UCNPs-CW and NIR irradiation in controllable DOX release from the micelle.

NO can inhibit P-glycoprotein mediated efflux of drug from target cells [34–36]. Thus nitroglycerin (NG), which can react with GSH for *in situ* NO generation [32,33], was also encapsulated in the hydrophobic micellar core. The generation of NO was verified with 3-amino-4-aminomethyl-2′,7′-difluorescein (DAF-FM), a non-fluorescent molecule that reacts with NO to produce strong emission at 522 nm [35], and quantified with NO detection kit. UCNPs-CW/NG@P-DASA was mixed with 50 μM DAF-FM and 10 mM GSH, and exposed to 808-nm light irradiation for 5 min. DAF-FM characteristic emission peak at 522 nm was observed from the mixture solution, and the fluorescence intensity continuously increased according to time (Fig. 2D), indicating the efficient generation of NO due to 5-min NIR exposure. The generated NO concentration was calculated as 725 nM at 30 min in the presence of NIR irradiation (Fig. 2E, red line). In the absence of 808-nm irradiation or GSH presence, the mixture solution barely showed NO generation (Fig. S5F and Fig. S5G; Fig. 2F, red line). Similarly, the micelle of NG@P-DASA also showed very weak DAF-FM fluorescence even in the presence of NIR exposure and GSH (Fig. S5H), indicating the negligible NO generation without UCNPs-CW. Additionally, the co-encapsulation of DOX didn't affect the capability of NO generation for micelle, and UCNPs-CW/NG/DOX@P-DASA demonstrated similar level of NO generation compared with UCNPs-CW/NG@P-DASA) (Fig. S5I). These results demonstrated the efficient NO generation capability of UCNPs-CW/NG@P-DASA.

3.3. Stability of the micelle

The size of UCNPs-CW/NG/DOX@P-DASA micelle showed little variation during 24-h incubation in PBS and PBS containing 10% fetal bovine serum (FBS) with stable PDI values (Fig. S6A and S6B), indicating good size stability. Additionally, the serum stability was examined with the DOX leakage in 10% FBS buffer in the absence of NIR irradiation according to time. The leakage of DOX was quantified by measuring the fluorescence intensity of supernatants at 592 nm, which remained below 10% even after 12 h-incubation (Fig. S6C), proving the satisfactory stability of UCNPs-CW/NG/DOX@P-DASA during drug delivery process.

3.4. Specific cellular internalization and internalization pathway

The specific cellular internalization was achieved by labelling FA at the hydrophilic end of P-DASA. After incubation with UCNPs-CW/NG/DOX@P-DASA for 6 h, MCF-7/ADR cells, which overexpresses FA receptors on cell membrane, showed obvious characteristic upconversion emission of UCNPs-CW under 808-nm excitation, while MCF-10a cells without FA receptor displayed negligible fluorescence (Fig. S7). Moreover, the pretreatment of MCF-7/ADR cells with excess FA highly suppressed the internalization of UCNPs-CW/NG/DOX@P-DASA (Fig. S7). These results demonstrated an FA-mediated internalization process.

To evaluate the internalization pathway of UCNPs-CW/NG/DOX@P-DASA into MCF-7/ADR cells, different inhibitors, such as NaN_3, sucrose, genistein and wortmannin, were employed to selectively block relevant internalization processes [39,40]. MCF-7/ADR cells were firstly treated with these inhibitors, and then incubated with Cy3 labelled $UCNPs_{Cy3}$-CW@P-DASA for 6 h to detect the fluorescence intensities of Cy3 in cells through flow cytometric assay. These inhibitors treated cells exhibited 62.5%, 49.1%, 26.9% and negligible suppression to $UCNPs_{Cy3}$-CW@P-DASA uptake, respectively (Fig. S8A), indicating that the internalization of the micelle underwent a mixed pathway of energy-dependent and clathrin-mediated endocytosis, and sort of caveolae-mediated endocytosis.

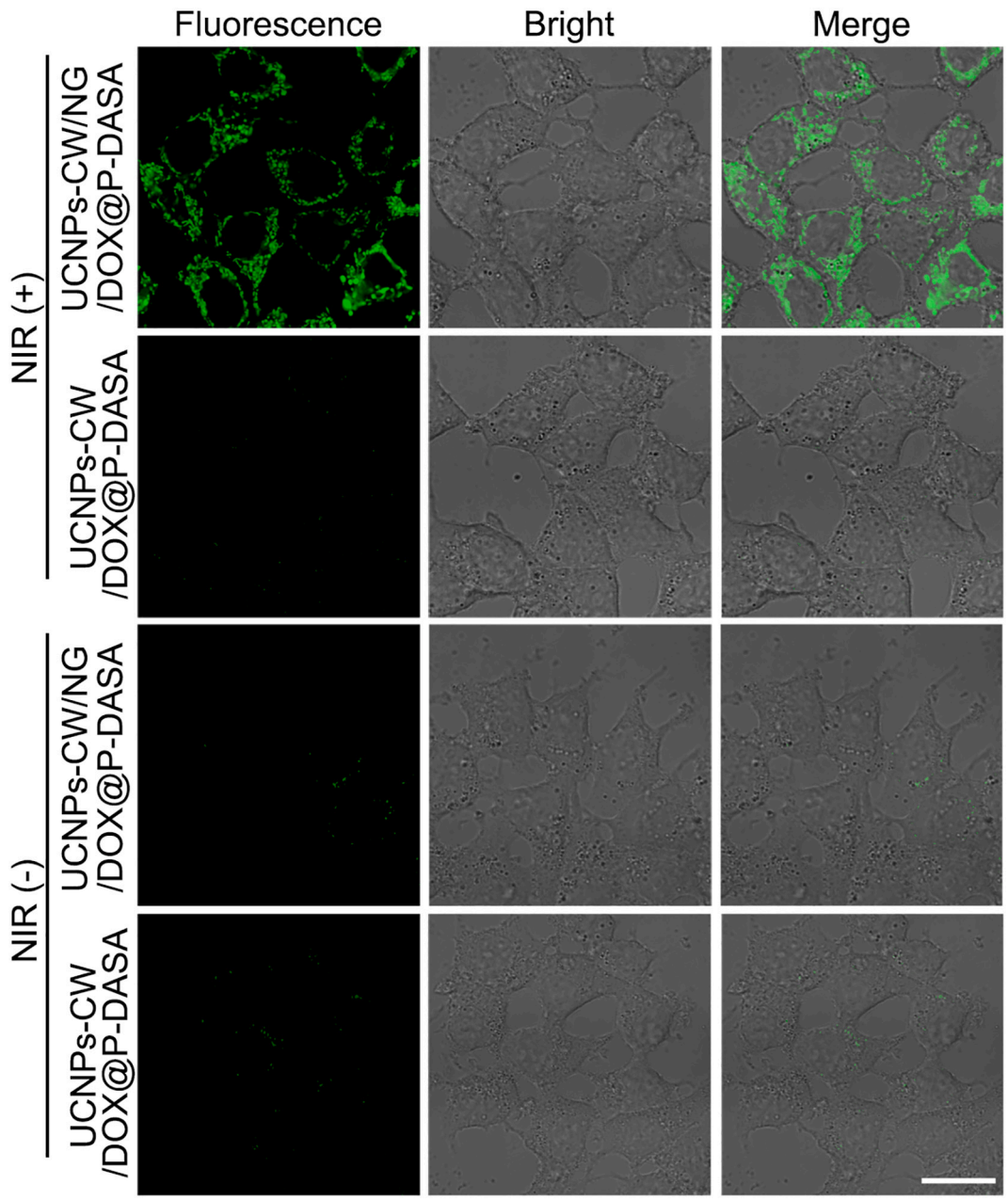

Fig. 4. CLSM images of micelle or UCNPs-CW/DOX@P-DASA treated MCF-7/ADR cells after staining with DAF-FM diacetate and then NIR irradiation or not (scale bar: 25 μm).

3.5. Intracellular DOX release and NO generation

The NIR-light responsive intracellular release of DOX was investigated through monitoring the intracellular distribution of DOX and UCNPs-CW. MCF-7/ADR cells were incubated with the micelle for 6 h, subsequently irradiated with 808-nm light (2 W cm^{-2}) for 5 min, and the CLSM images were taken after continuous 25 min incubation in cell culture medium. The fluorescence of DOX showed nuclear accumulation clearly and displayed good overlap with nuclear dye DAPI, while the UCNPs-CW emission was mostly localized in cytoplasm (Fig. 3, NIR(+)), indicating the efficient drug release upon micelle disassembly. In comparison, the good overlap of red (UCNPs-CW) and green (DOX) fluorescence was observed in the cytoplasm in the absence of NIR irradiation (Fig. 3, NIR(−)), indicating that the DOX was remained in the micelle along with UCNPs-CW.

The intracellular generation of NO was examined using DAF-FM diacetate, which reacts with intracellular esterase to produce DAF-FM, and demonstrates intracellular green fluorescence at 522 nm [39]. MCF-7/ADR cells were incubated with UCNPs-CW/NG/DOX@P-DASA, exposed under 5-min NIR irradiation, and displayed obvious intracellular green fluorescence after continuous 25-min incubation (Fig. 4, NIR (+), UCNPs-CW/NG/DOX@P-DASA), indicating the efficient release of NG and intracellular NO generation. In comparison, UCNPs-CW/DOX@P-DASA incubated cells did not show intracellular characteristic fluorescence upon NIR irradiation (Fig. 4, NIR(+), UCNPs-CW/DOX@P-DASA). Little characteristic fluorescence was observed either for UCNPs-CW/NG/DOX@P-DASA and UCNPs-CW/DOX@P-DASA treated cells in the absence of NIR irradiation (Fig. 4, NIR(−)).

3.6. Cellular cytotoxicity and therapeutic effect

The cytotoxicity of UCNPs-CW/NG/DOX@P-DASA to MCF-7/ADR

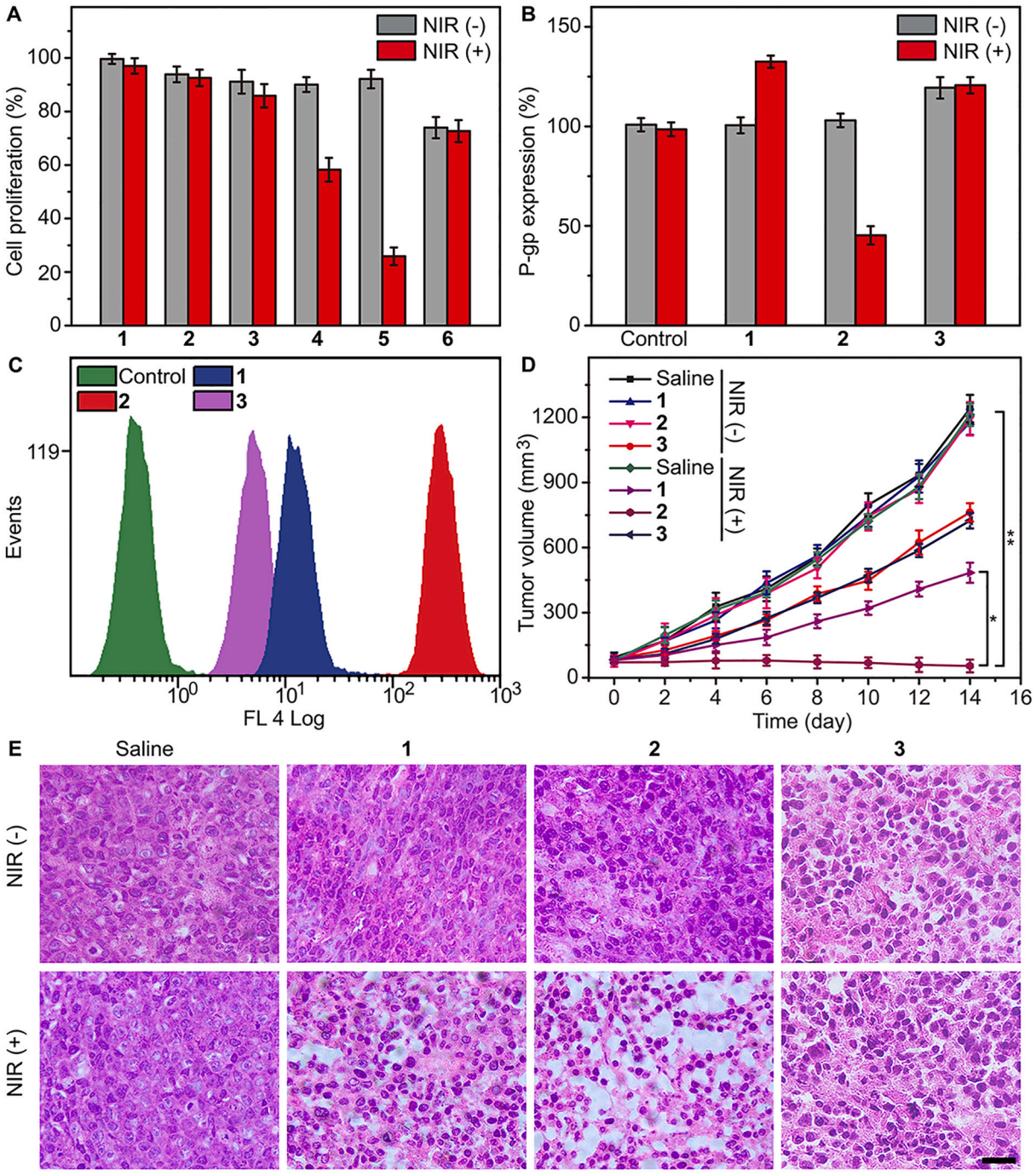

Fig. 5. (A) Relative cell proliferation rates of MCF-7/ADR cells (1) and UCNPs-CW@P-DASA (2), UCNPs-CW/NG@P-DASA (3), UCNPs-CW/DOX@P-DASA (4), UCNPs-CW/NG/DOX@P-DASA (5) or DOX (6) treated MCF-7/ADR cells in the presence and absence of 5-min NIR irradiation and continuous incubaiton of 24-h. (B) P-gp expression levels of MCF-7/ADR cells (control) and UCNPs-CW/DOX@P-DASA (1), UCNPs-CW/NG/DOX@P- DASA (2) or DOX (3) treated MCF-7/ADR cells in the presence and absence of 5-min NIR irradiation and continuous incubaiton of 12 h. The data error bars indicate means ± SD ($n = 3$). (C) Flow cytometric assays of MCF-7/ADR cells (control) and UCNPs-CW/DOX@P-DASA (1) or UCNPs-CW/NG/DOX@P-DASA (2) or DOX (3) treated MCF-7/ADR cells in the presence of 5-min NIR irradiation and 6-h incubation. (D) Tumor volume changes of mice and (E) histological observations of tumor tissues treated with saline, UCNPs-CW/DOX@P-DASA (1), UCNPs-CW/NG/DOX@P-DASA (2) or DOX (3) in the presence and absence of 5-min NIR irradiation. The data error bars indicate means ± SD ($n = 5$). *$P <$ 0.01 and **$P < 0.005$ with two-tailed Student's t-test. Scale bar: 50 μm.

cells was evaluated through 3-(4,5-dimethylthiazol-2-yl)-2-diphenyltetrazolium bromide (MTT) assay. After incubating with the micelle for 6 h, MCF-7/ADR cells showed over 90% of viability even at the micelle concentration as high as 500 μg mL^{-1} (Fig. S8B), demonstrating the non-cytotoxicity of this micelle. The good biocompatibility of the micelle was further confirmed by their little effect on cell proliferation in the absence of NIR irradiation (Fig. 5A, NIR (−) in column 5) or NG/DOX loading (Fig. 5A, column 2). 5-min NIR light irradiation greatly lowered the proliferation rate of the micelle treated MCF-7/ADR cells to 25.9% (Fig. 5A, NIR (+) in column 5), proving better therapeutic efficiency of NIR light fast ignited micelle than free DOX treatment (Fig. 5A, column 6). UCNPs-CW/DOX@P-DASA incubated MCF-7/ADR cells demonstrated limited therapeutic effect with only 58.4% of cell proliferation rate in the absence of NG (Fig. 5A, NIR (+) in column 4), and UCNPs-

CW/NG@P-DASA with only NG encapsulation barely demonstrated suppression to cell proliferation due to its relatively insufficient concentration level [41,42]. (Fig. 5A, NIR (+) in column 3), indicating the contribution of intracellular NO generation to therapeutic effect due to the suppression of P-gp mediated drug efflux in tumor cells.

To further clarify the mechanism of NO-boosted tumor therapy, the P-gp expression level in MCF-7/ADR cells was analyzed through enzyme-linked immunosorbent assay (ELISA). In the absence of NIR irradiation, the expression level of P-gp did not display obvious change after incubating cells with UCNPs-CW/NG/DOX@P-DASA, while 5-min NIR irradiation caused remarkable decrease of P-gp expression to 53.1% (Fig. 5B, column 2). However, UCNPs-CW/DOX@P-DASA and free DOX even enhanced the P-gp expression to some extent after NIR irradiation, compared to its original expression level (Fig. 5B, column 1 and column 3), which was probably ascribed to the stimulation of released DOX [38].

The suppression of drug efflux resulted efficient intracellular DOX accumulation for cell killing. The intracellular DOX accumulation was clearly demonstrated *via* flow cytometry for the micelle incubated MCF-7/ADR cells. It showed the strongest intracellular fluorescence of DOX with 5-min NIR irradiation, compared with free DOX or UCNPs-CW/DOX@P-DASA incubated MCF-7/ADR cells (Fig. 5C).

The superiority of the micelle for killing MCF-7/ADR cells was further verified by detecting the cell apoptosis rates with Annexin V-FITC/propidium iodide (PI) apoptosis assay kit. After 5-min NIR light irradiation and continuous 25-min incubation, UCNPs-CW/NG/DOX@P-DASA treated MCF-7/ADR cells showed a cell apoptosis rate of 76.2%, higher than that of 43.1% or 28.5% for the cells treated with UCNPs-CW/DOX@P-DASA or free DOX, while the cell apoptosis rates were only 11.6% and 9.0% for UCNPs-CW/NG/DOX@P-DASA and UCNPs-CW/DOX@P-DASA treated MCF-7/ADR cells respectively in the absence of NIR light irradiation (Fig. S8C).

3.7. *In vivo* antitumor effect

The *in vivo* antitumor therapeutic efficiency of the micelle was verified with nude mice bearing MCF-7/ADR xenograft tumor. The biodistribution of $UCNPs_{Cy3}$-CW@P-DASA showed good accumulation into tumor sites at 4 h after intravenous injection with little nonspecific fluorescence at liver/spleen (Fig. S9), therefore 4 h was chosen as the time point to apply light irradiation. On the contrary, non-targeted micelle $UCNPs_{Cy3}$-CW@P-DASA' in the absence of FA showed much weaker Cy3 fluorescence at tumor sites with stronger nonspecific fluorescence in liver and spleen (Fig. S10). Saline, UCNPs-CW/DOX@P-DASA and UCNPs-CW/NG/DOX@P-DASA were intravenously injected into different groups of mice respectively. In the presence of 5-min NIR irradiation, the UCNPs-CW/NG/DOX@P-DASA injected group demonstrated the superior inhibition towards tumor growth (Fig. 5D, NIR(+) in line 2 and Fig. S11, UCNPs-CW/NG/DOX@P-DASA, NIR(+)). It was more effective than UCNPs-CW/DOX@P-DASA or DOX injected group (Fig. S11, UCNPs-CW/DOX@P-DASA, NIR(+); DOX, NIR(+)). The high therapeutic efficiency of the micelle was attributed to the NIR quick disruption of the micelle in accompany with the efficient release of DOX, and the simultaneous inhibition of drug efflux. Furthermore, the tumor tissues from the micelle treated mice showed massive cell atrophy with more prominent apoptosis of cells in the presence of NIR irradiation (Fig. 5E), confirming *in vivo* anticancer therapeutic effect of the micelle. The micelle treated mice did not show obvious variation in the body weight during the 14 days of therapeutic treatment (Fig. S12), and the histological analysis of mice heart, liver, spleen, lung and kidney did not also show obvious pathological abnormality (Fig. S13), which verified the *in vivo* biocompatibility of the as presented micelle with little side effects and toxicity.

4. Conclusion

Taking advantage of the capability of upconversion emission of UCNPs, NIR light-responsive nanocarriers have been extensively developed for drug delivery recently. However, most current strategies require extended period of NIR light irradiation over hours with sluggish drug release, which complicates treatment process and brings additional thermal injuries to healthy cells and tissues. To solve this problem, here we coupled Er^{3+} doped UCNPs with self-assembled micelle to develop a NIR light fast ignited micelle for quick drug release. Only 5-min NIR irradiation caused the hydrophilicity conversion of micelle component P-DASA, and resulted the complete disruption of the micelle with quick and sufficient DOX release of 83.7% in 30 min. The simultaneous intracellular NO generation inhibited the P-gp expression and further improved therapeutic efficiency. The as-presented NIR light fast ignited micelle demonstrated high anticancer efficiency for both cellular and *in vivo* experiments, implying great promise in precise tumor therapy and clinical therapeutic applications.

Credit author statement

Yue Zhang: Designing strategies, Performing experiments, Analyzing data, Writing manuscript.

Xiaobo Zhang: Performing experiments.

Weiwei Chen: Performing experiments.

Yuling He: Performing experiments.

Ying Liu: Supervision, Designing strategies, Writing and revising manuscript.

Huangxian Ju: Supervision, Designing strategies, Revising manuscript.

Acknowledgements

We gratefully acknowledge the National Natural Science Foundation of China (21635005, 21974064, 22022405, 22004068, 21890741, 21771103), Natural Science Foundation of Jiangsu Province for distinguished Young Scholars (BK20200010), Specially-appointed Professor Foundation and Program for Innovative Talents and Entrepreneurs of Jiangsu Province, State Key Laboratory of Analytical Chemistry for Life Science (5431ZZXM2003).

Appendix A. Supplementary data

Supplementary data to this article can be found online at https://doi.org/10.1016/j.jconrel.2021.06.028.

References

[1] F. Seidi, R. Jenjob, D. Crespy, Designing smart polymer conjugates for controlled release of payloads, Chem. Rev. 118 (2018) 3965–4036.
[2] Y. Wang, S. Li, P. Zhang, H. Bai, L. Feng, F. Lv, L. Liu, S. Wang, Photothermal-responsive conjugated polymer nanoparticles for remote control of gene expression in living cells, Adv. Mater. 30 (2018) 1705418.
[3] Y. Matsumura, T. Hamaguchi, T. Ura, K. Muro, Y. Yamada, Y. Shimada, K. Shirao, T. Okusaka, H. Ueno, M. Ikeda, N. Watanabe, Phase I clinical trial and pharmacokinetic evaluation of NK911, a micelle-encapsulated doxorubicin, Br. J. Cancer 91 (2004) 1775–1781.
[4] M. Baba, Y. Matsumoto, A. Kashio, H. Cabral, N. Nishiyama, K. Kataoka, T. Yamasoba, Micellization of Cisplatin [NC-6004] reduces its ototoxicity in Guinea Pigs, J. Control. Release 157 (2012) 112–117.
[5] R. Wei, X. Gong, H. Lin, K. Zhang, A. Li, K. Liu, H. Shan, X. Chen, J. Gao, Versatile octapod-shaped hollow porous manganese[II] oxide nanoplatform for real-time visualization of cargo delivery, Nano Lett. 19 (2019) 5394–5402.
[6] C. Yao, Y. Li, Z. Wang, C. Song, X. Hu, S. Liu, Cytosolic NQO1 enzyme-activated near-infrared fluorescence imaging and photodynamic therapy with polymeric vesicles, ACS Nano 14 (2020) 1919–1935.
[7] H. Cai, X. Dai, X. Wang, P. Tan, L. Gu, Q. Luo, X. Zheng, Z. Li, H. Zhu, H. Zhang, Z. Gu, Q. Gong, K. Luo, A nanostrategy for efficient imaging-guided antitumor therapy through a stimuli-responsive branched polymeric Prodrug, Adv. Sci. 7 (2020) 1903243.

[8] B. Ma, H. Xu, W. Zhuang, Y. Wang, G. Li, Y. Wang, Reactive oxygen species responsive theranostic nanoplatform for two-photon aggregation-induced emission imaging and therapy of acute and chronic inflammation, ACS Nano 14 (2020) 5862–5873.
[9] M. Zhou, H. Huang, D. Wang, H. Lu, J. Chen, Z. Chai, S.Q. Yao, Y. Hu, Light-triggered PEGylation/dePEGylation of the nanocarriers for enhanced tumor penetration, Nano Lett. 19 (2019) 3671–3675.
[10] C. Brieke, F. Rohrbach, A. Gottschalk, G. Mayer, A. Heckel, Light-controlled tools, Angew. Chem. Int. Ed. 51 (2012) 8446–8476.
[11] X. Zhu, J. Zhang, J. Liu, Y. Zhang, Recent progress of rare-earth doped upconversion nanoparticles: synthesis, optimization, and applications, Adv. Sci. 6 (2019) 1901358.
[12] H. Li, X. Wang, T.Y. Ohulchanskyy, G. Chen, Lanthanide-doped near-infrared nanoparticles for biophotonics, Adv. Mater. 33 (2021) e2000678.
[13] J. Zhao, Y. Li, M. Yu, Z. Gu, L. Li, Y. Zhao, Time-resolved activation of pH sensing and imaging in vivo by a remotely controllable DNA nanomachine, Nano Lett. 20 (2020) 874–880.
[14] H. Chu, J. Zhao, Y. Mi, Y. Zhao, L. Li, Near-infrared light-initiated hybridization chain reaction for spatially and temporally resolved signal amplification, Angew. Chem. Int. Ed. 58 (2019) 14877–14881.
[15] J. Zhao, H. Chu, Y. Zhao, Y. Lu, L. Li, A NIR light gated DNA nanodevice for spatiotemporally controlled imaging of microRNA in cells and animals, J. Am. Chem. Soc. 141 (2019) 7056–7062.
[16] J. Zhao, J. Gao, W. Xue, Z. Di, H. Xing, Y. Lu, L. Li, Upconversion luminescence-activated DNA nanodevice for ATP sensing in living cells, J. Am. Chem. Soc. 140 (2018) 578–581.
[17] Z. Di, B. Liu, J. Zhao, Z. Gu, Y. Zhao, L. Li, An orthogonally regulatable DNA nanodevice for spatiotemporally controlled biorecognition and tumor treatment, Sci. Adv. 6 (2020) eaba9381.
[18] H. Chu, J. Zhao, Y. Mi, Z. Di, L. Li, NIR-light-mediated spatially selective triggering of anti-tumor immunity via upconversion nanoparticle-based immunodevices, Nat. Commun. 10 (2019) 2839.
[19] B. Yan, J.C. Boyer, N.R. Branda, Y. Zhao, Near-infrared light-triggered dissociation of block copolymer micelles using upconverting nanoparticles, J. Am. Chem. Soc. 133 (2011) 19714–19717.
[20] C. Yao, P. Wang, X. Li, X. Hu, J. Hou, L. Wang, F. Zhang, Near-infrared-triggered azobenzene-liposome/upconversion nanoparticle hybrid vesicles for remotely controlled drug delivery to overcome cancer multidrug resistance, Adv. Mater. 28 (2016) 9341–9348.
[21] C. Liu, Y. Zhang, M. Liu, Z. Chen, Y. Lin, W. Li, F. Cao, Z. Liu, J. Ren, X. Qu, A NIR-controlled cage mimicking system for hydrophobic drug mediated cancer therapy, Biomaterials 139 (2017) 151–162.
[22] J. Zhou, Z. Liu, F. Li, Upconversion nanophosphors for small-animal imaging, Chem. Soc. Rev. 41 (2012) 1323–1349.
[23] S. Wilhelm, Perspectives for upconverting nanoparticles, ACS Nano 11 (2017) 10644–10653.
[24] G. Chen, R. Jaskula-Sztul, C.R. Esquibel, I. Lou, Q. Zheng, A. Dammalapati, A. Harrison, K.W. Eliceiri, W. Tang, H. Chen, S. Gong, Neuroendocrine tumor-targeted upconversion nanoparticle-based micelles for simultaneous NIR-controlled combination chemotherapy and photodynamic therapy, and fluorescence imaging, Adv. Funct. Mater. 27 (2017) 1604671.
[25] Q. Zou, P. Huang, W. Zheng, W. You, R. Li, D. Tu, J. Xu, X. Chen, Cooperative and non-cooperative sensitization upconversion in lanthanide-doped $LiYbF_4$ nanoparticles, Nanoscale 9 (2017) 6521–6528.
[26] Y. He, S. Guo, L. Wu, P. Chen, L. Wang, Y. Liu, H. Ju, Near-infrared boosted ROS responsive SiRNA delivery and cancer therapy with sequentially peeled upconversion nano-onions, Biomaterials 225 (2019) 119501.
[27] M. Tang, X. Zhu, Y. Zhang, Z. Zhang, Z. Zhang, Q. Mei, J. Zhang, M. Wu, J. Liu, Y. Zhang, Near-infrared excited orthogonal emissive upconversion nanoparticles for imaging-guided on-demand therapy, ACS Nano 13 (2019) 10405–10418.
[28] X. Sun, J. Sun, B. Dong, G. Huang, L. Zhang, W. Zhou, J. Lv, X. Zhang, M. Liu, L. Xu, X. Bai, W. Xu, Y. Yang, X. Song, H. Song, Noninvasive temperature monitoring for dual-modal tumor therapy based on lanthanide-doped up-conversion nanocomposites, Biomaterials 201 (2019) 42–52.
[29] T. Senthilkumar, L. Zhou, Q. Gu, L. Liu, F. Lv, S. Wang, Conjugated polymer nanoparticles with appended photo-responsive units for controlled drug delivery, release, and imaging, Angew. Chem. Int. Ed. 57 (2018) 13114–13119.
[30] S. Helmy, F.A. Leibfarth, S. Oh, J.E. Poelma, C.J. Hawker, J. Read de Alaniz, Photoswitching using visible light: a new class of organic photochromic molecules, J. Am. Chem. Soc. 136 (2014) 8169–8172.
[31] X. Zhang, W. Chen, X. Xie, Y. Li, D. Chen, Z. Chao, C. Liu, H. Ma, Y. Liu, H. Ju, Boosting luminance energy transfer efficiency in upconversion nanoparticles with an energy-concentrating zone, Angew. Chem. Int. Ed. 58 (2019) 12117–12122.
[32] A. Prasad, N.P. Andrews, F.A. Padder, M. Husain, A.A. Quyyumi, Glutathione reverses endothelial dysfunction and improves nitric oxide bioavailability, J. Am. Coll. Cardiol. 34 (1999) 507–514.
[33] K.E. Hill, R.W. Hunt, R. Jones, R.L. Hoover, R.F. Burk, Metabolism of nitroglycerin by smooth muscle cells: involvement of glutathione and glutathione S-transferase, Biochem. Pharmacol. 43 (1992) 561–566.
[34] M. Chen, F. Song, Y. Liu, J. Tian, C. Liu, R. Li, Q. Zhang, A dual pH-sensitive liposomal system with charge-reversal and NO generation for overcoming multidrug resistance in cancer, Nanoscale 11 (2019) 3814–3826.
[35] V.G. Deepagan, H. Ko, S. Kwon, N.V. Rao, S.K. Kim, W. Um, S. Lee, J. Min, J. Lee, K.Y. Choi, S. Shin, M. Suh, J.H. Park, Intracellularly activatable nanovasodilators to enhance passive cancer targeting regime, Nano Lett. 18 (2018) 2637–2644.
[36] L. Wang, Y. Chang, Y. Feng, X. Li, Y. Cheng, H. Jian, X. Ma, R. Zheng, X. Wu, K. Xu, H. Zhang, Nitric oxide stimulated programmable drug release of nanosystem for multidrug resistance cancer therapy, Nano Lett. (2019) 6800–6811.
[37] Y. Zhang, Z. Yu, J. Li, Y. Ao, J. Xue, Z. Zeng, X. Yang, T.T. Tan, Ultrasmall-superbright neodymium-upconversion nanoparticles via energy migration manipulation and lattice modification: 808 nm-activated drug release, ACS Nano 11 (2017) 2846–2857.
[38] O. Rifaie-Graham, S. Ulrich, N.F.B. Galensowske, S. Balog, M. Chami, D. Rentsch, J. R. Hemmer, J. Read de Alaniz, L.F. Boesel, N. Bruns, Wavelength-selective light-responsive DASA-functionalized polymersome nanoreactors, J. Am. Chem. Soc. 140 (2018) 8027–8036.
[39] K. Ren, Y. Zhang, X. Zhang, Y. Liu, M. Yang, H. Ju, In situ SiRNA assembly in living cells for gene therapy with MicroRNA triggered cascade reactions templated by nucleic acids, ACS Nano 12 (2018) 10797–10806.
[40] K. Ren, Y. Liu, J. Wu, Y. Zhang, J. Zhu, M. Yang, H. Ju, A DNA dual lock-and-key strategy for cell-subtype-specific SiRNA delivery, Nat. Commun. 7 (2016) 13580.
[41] S.C. Wu, C.Y. Lu, Y.L. Chen, F.C. Lo, T.Y. Wang, Y.J. Chen, S.S. Yuan, W.F. Liaw, Y. M. Wang, Water-soluble dinitrosyl iron complex (DNIC): a nitric oxide vehicle triggering cancer cell death via apoptosis, Inorg. Chem. 55 (2016) 9383–9392.
[42] Y. Kang, J. Kim, J. Park, Y.M. Lee, G. Saravanakumar, K.M. Park, W. Choi, K. Kim, E. Lee, C. Kim, W.J. Kim, Tumor vasodilation by N-heterocyclic carbene-based nitric oxide delivery triggered by high-intensity focused ultrasound and enhanced drug homing to tumor sites for anti-cancer therapy, Biomaterials 217 (2019) 119297.